This is the accepted manuscript made available via CHORUS. The article has been published as:

Structure and physical properties of SrNiRu_{5}O_{11} single crystals: An R-type ferrite based on ordered kagome nets

L. Shlyk, L. E. De Long, and R. Niewa

Phys. Rev. B **95**, 024433 — Published 30 January 2017

DOI: 10.1103/PhysRevB.95.024433

Structure and Physical Properties of $SrNiRu_5O_{11}$ Single Crystals: A New R-type Ferrite Based on Ordered Kagome Nets

L. Shlyk[1], L.E. De Long[2], and R. Niewa[1]

[1]Universität Stuttgart, Institut für Anorganische Chemie, Pfaffenwaldring 55, 70569 Stuttgart, Germany

[2]University of Kentucky, Department of Physics and Astronomy, CP177, 505 Rose Street, Lexington KY, USA 40506-0055

Abstract. Single crystals of the R-type ferrite $SrNiRu_5O_{11}$ were grown from a chloride flux. The hexagonal crystal structure contains ruthenium located on distorted Kagomé nets. The low-temperature DC magnetic susceptibilities, ($\chi_\perp$ and $\chi_{/\!/}$, perpendicular and parallel to the ***c***-axis, respectively) diverge as $T^{-0.3}$, and do not exhibit any indication of long-range magnetic order down to 4.5 K. The electrical resistivity varies as $T^{1.6}$ below 40 K, which is typical of non-Fermi liquids, and may originate from a competition between residual magnetic interactions among Ni^{2+} (S = 1) spins and geometrical frustration on the two-dimensional Kagomé lattice of Ru^{3+} (S = ½) spins. The transverse magnetoresistivity ρ_{xy} at constant temperature T = 5 K for current (***J***) - magnetic field (***H***) configurations, ***J*** ⊥ ***H*** || ***c***-axis and ***J*** || ***H*** ⊥ ***c***-axis, reveals no anomalous contribution, which is typical of non-magnetic materials. Fits of the specific heat data below 10 K require a dominant, but unusual electronic term of the form $C_{el} = \gamma T^{1.2}$, which is expected for massless Dirac fermion states in topological insulators or spin-liquid phases.

Keywords: Ruthenates, Kagome Net, Magnetic Properties, Transport Properties, Spin Liquid, Frustration.

1. Introduction

Ruthenium oxides have been intensively investigated over the last two decades as a very interesting class of transition metal oxides with unusual physical properties **[1]**. One of the most important features of 4*d* transition metal oxides is the large spatial extent of their 4*d*-electron orbitals, which favors their greater delocalization compared to their 3*d* counterparts, which leads to increased hybridization of transition metal and oxygen states, and modifies crystalline-electric field interactions. These features are known to be responsible for a variety of exotic magnetic properties in ruthenium oxides **[2]**.

Previously, we have studied ternary ruthenium ferrites with chemical formula $(Ba,Sr)T_{2\pm x}Ru_{4\mp x}O_{11}$ (T = Fe, Co, Mn), which crystallize in the hexagonal R-type ferrite structure **[3-7]**, which contains a Kagomé substructure of mixed occupancy by Ru and transition element T, as shown in **Fig. 1**. Layers of edge-sharing $M(2)O_6$ octahedra form a Kagomé net within the ***ab***-plane; and the Kagomé planes are connected along [001] by face-sharing $M(1)O_6$ octahedra and $M(3)O_5$ trigonal bipyramids. It is important to note that the variable occupation of octahedrally coordinated M(1) and M(2) sites by 3d elements and 4d ruthenium generate large homogeneity ranges, while the M(3) sites with trigonal-pyramidal coordination are exclusively occupied by 3d elements. The substitution of 3d elements for 4d ruthenium within large homogeneity ranges permits precise control of magnetic order (including attainment of unusually high Curie temperatures $T_C \sim 490$ K), a narrow semiconducting gap ($\Delta \sim 0.1$ eV) and a sizeable anomalous Hall effect, making these materials very attractive for spintronic applications **[4]**. Furthermore, the mixed occupancy of the M(2) sites by Ru and *M* in the frustrated Kagomé plane gives rise to exotic physical phenomena such as non-zero scalar chirality **[6]**, which has attracted increasing attention due to its potential exploitation in applications.

In this paper we report electric, magnetic and thermodynamic properties of $SrNiRu_5O_{11}$ single crystals, which is a new representative of the broad family of ternary ruthenium ferrites. In contrast to most previously studied members of the R-type ferrites, no 3d/4d atomic disorder is observed on the M(2)/M(3) sites of $SrNiRu_5O_{11}$. However, the Kagomé net is distorted due formation of Ru–Ru dumbbells via metal-metal bonding in $SrNiRu_5O_{11}$ and $BaZnRu_5O_{11}$ **[8]**. Together with the compounds $(Ba,Sr)TRu_5O_{11}$ with T = Li, Zn and Cu **[8-10]**, $SrNiRu_5O_{11}$ constitutes an uncommon example of an ordered structure within the R-type ferrite family. Our results verify that such an ordered structure enhances magnetic frustration within the Kagomé planes, and allows one to study a proximate quantum critical state that generates non-Fermi liquid (NFL) behavior at low temperatures (as demonstrated by $BaZnRu_5O_{11}$ **[10]**).

2. Experimental Details

The DC magnetization M of oriented single crystals was measured over a temperature range 5 K $\leq T \leq$ 300 K in applied magnetic fields $0 \leq \mu_o H \leq 5$ T using a Quantum Design MPMS5 SQUID Magnetometer. Longitudinal and transverse magnetoresistivities, $\rho_{xx}(T)$ and $\rho_{xy}(H,T)$, respectively, were measured using a DC four-probe setup with currents $\boldsymbol{J}$ directed in the ***ab***-plane with magnitudes 5 mA $\leq J \leq$ 20 mA. The specific heats of several crystals were measured over a temperature range 0.35 K – 50 K using a Quantum Design PPMS9 System.

3. Results and Discussion

3.1. Crystal Structure and Composition

We have previously reported on the growth of $SrNiRu_5O_{11}$ single crystals (**Fig. 2**) from $SrCl_2$ flux, and their crystal structure determination **[8]**. According to microprobe chemical analysis and x-ray structure refinements, the composition is well represented by $SrNiRu_5O_{11}$ with no

indication of any significant homogeneity range. However, $SrNiRu_5O_{11}$ exhibits a doubled unit cell parameter *a* (*a* = 11.7374(2) Å, *c* = 13.2088(4) Å) with a lower space group symmetry, $P6_3/m$, as compared to the $P6_3/mmc$ R-type hexagonal unit cell **[8]**. **Figure 1** shows a section of the smaller R-type substructure, which is sufficient for discussion of the metal atom sites. Ni atoms are restricted to the trigonal bipyramids of oxide ions, but randomly occupy either one or the other of the two adjacent tetrahedrally coordinated sites within the bipyramids. The Ru(2) sites have octahedral coordination by oxygen, and form distorted Kagomé nets, whereas the Ru(1) occupy face-sharing, double-octahedra that connect the Kagomé nets along the [001] direction.

3.2. Magnetic and Transport Properties

The magnetic species in $SrNiRu_5O_{11}$ include Ru^{3+} (S = ½) ions that form a Kagomé sublattice in the ***ab***-planes, which are separated from adjacent Kagomé planes by magnetic Ni^{2+} (S = 1) and non-magnetic Ru^{4+} (Ru(1), S = 0) ions. The proposed spin configurations for Ru and Ni are based on the crystal structure refinements, which suggest a $3d^8$ electron configuration for the Ni (M(3) site), $4d^5$ for the Ru(2) (M(2) site), and $4d^4$ for the Ru(1) (M(1) site) **[9]**. We assume Ru(1) to be in a low-spin state (Ru^{4+}, S = 0) since neutron diffraction investigations performed on Co- and Mn-bearing ferrites consistently indicate there is no magnetic moment on this site **[10,11]**.

Our high-temperature magnetic susceptibility data are shown in the insets to **Figs. 3** and **4**. The inverse field-cooled (FC) DC susceptibility for $\boldsymbol{H} \perp \boldsymbol{c}$ (**Fig. 3** inset) presents a change in slope near 60 K and a near-linear temperature dependence above 100 K. A Curie-Weiss fit of the data in the temperature interval 100 K < T < 300 K gives a Curie-Weiss temperature θ_p = –150 K and an effective magnetic moment $\mu_{eff} \approx 4.7\mu_B$. The susceptibility of single-crystal $SrNiRu_5O_{11}$ is anisotropic and about two times higher for $\boldsymbol{H} \parallel \boldsymbol{c}$ than for $\boldsymbol{H} \perp \boldsymbol{c}$. Above 100 K,

$\chi_{//}$ follows a Curie-Weiss law with $\theta_p = -69$ K, and $\mu_{eff} = 4.9\ \mu_B$ (**Fig. 4** inset). The negative θ_p value is consistent with the dominance of antiferromagnetic interactions between room temperature and approximately 100 K. An estimation of the theoretical effective magnetic moment can be obtained using an expression $\mu_{eff} = [n_1\mu^2(Ni^{2+}) + n_2\mu^2(Ru^{3+}) + n_3\mu^2(Ru^{4+})]^{1/2}$, where n_1, n_2 and n_3 are the molar fractions of Ni^{2+}, Ru^{3+} and Ru^{4+}, respectively. Insertion of the effective magnetic moments μ for spin-only Ru^{3+}($S = 1/2$), Ru^{4+} ($S = 0$) and Ni^{2+} ($S = 1$) yields a value for the net effective moment, $\mu_{eff} = 4.1\mu_B$, which is in reasonable agreement with the experimental values. On the other hand, the experimental value of μ_{eff} is close to the range of the values typically observed for Ni^{2+} in high-spin complexes **[12]**, and suggests the presence of an orbital contribution. For example, in tetrahedral coordination, Ni^{2+} favors the $^3T_{1g}$ triplet state, which may be subject to spin-orbit coupling; these circumstances could lead to potential effective moments for Ni^{2+} lying in the range 3.5 to 4.2 μ_B **[12]**. It must be stressed that these calculated values of the effective magnetic moment are based on rough estimates that do not take into consideration strong spin-orbit interactions present in 4d transition metal oxides **[2]**.

The most important conclusion we draw from the low-temperature data for the magnetic susceptibility of single-crystal $SrNiRu_5O_{11}$ under a magnetic field of $H = 0.1$ T applied either parallel or perpendicular to the ***c***-axis (see **Figs. 3** and **4**, respectively) is that $\chi(T) \sim T^{-0.3}$ over a *one-order-of-magnitude* range of temperature. More precisely, the magnetic susceptibility follows a $T^{-0.33}$ dependence below 20 K for $\boldsymbol{H} \perp \boldsymbol{c}$, and a $T^{-0.26}$ dependence below 40 K for $\boldsymbol{H} \parallel \boldsymbol{c}$. This behavior of $SrNiRu_5O_{11}$ conflicts with simple Fermi liquid theory, where χ tends to a constant as $T \rightarrow 0$. The low-temperature divergence of the magnetic susceptibility suggests the existence of unusual magnetic excitations that differ from those of familiar Fermi liquids. On the other hand, a $T^{-0.3}$ power law can be attributed to NFL behavior that is associated with a nearby low-temperature quantum critical point (QCP) between paramagnetic and

magnetically ordered states **[13]**. The magnetization curves are non-linear at 5 K for both directions of the applied field, as shown in **Fig. 5**. A small hysteresis is observed when field is applied parallel to the ***c***-axis, suggesting weak ferromagnetic correlations. Above 130 K, the *M* vs. *H* loops are linear (**Fig. 6**). Note that the neutron diffraction investigations on metallic Mn- and Co-analogues indicate that M(3) sites always order with spins ferromagnetically aligned along the ***c***-axis **[10,11]**. This motivates our speculation that Ni^{2+} ions occupying M(3) sites are responsible for weak ferromagnetic correlations evident in the sample data below 130 K.

Our magnetic data for $SrNiRu_5O_{11}$ indicate this compound does not undergo long-range magnetic order down to 4.5 K, in contrast to the strong ferromagnetic order previously observed for $(Ba,Sr)T_{2\pm x}Ru_{4\mp x}O_{11}$ (T= Fe, Co, Mn) **[10,11]**. This result points to the presence of much stronger geometrical frustration in the Ni-bearing ferrite due to the reduced disorder on Ru(2) sites in the Kagomé planes.

Measurements of the Hall coefficient are a good alternative probe of the magnetization of ferromagnetic materials, since the Hall resistivity is expressed as

$$\rho_{xy} = R_0 H + 4\pi M R_s, \qquad \textbf{(1)}$$

where R_0 is the Hall coefficient resulting from the Lorentz force on the carriers, and R_s is the coefficient describing the anomalous Hall effect (AHE) that depends on the magnetization *M* and spin-orbit coupling **[14,15]**. In particular, ρ_{xy} has roughly the same field dependence as the magnetization in the ferromagnetic state below T_C. Moreover, a new "topological Hall effect" (THE) related to the spin chirality in non-coplanar spin configurations has been recently proposed **[16]**. In contrast with the conventional mechanism, the THE does not require any spin-orbit coupling, and arises solely from the Berry phase acquired by an electron moving in a smoothly varying magnetization **[17]**. A THE driven by spin chirality has been experimentally observed in ferromagnetic Co- and Mn-bearing ferrites **[6,11]**.

Ferromagnetic materials are not ideal for inducing a large THE, since strong ferromagnetic correlations tend to mask the THE when field is applied along the net magnetization of the sample. Although $SrNiRu_5O_{11}$ appears to be a paramagnetic semimetal, it could alternatively have an "all-in/all out" or "q = 0" planar spin configuration **[10]** with no net moment, in which case it might exhibit a THE in an external field that induces a non-coplanar (e.g., canted along the ***c*-**axis) spin configuration among the Ru ions residing on the Kagomé sublattice **[6]**.

We measured $\rho_{xy}(H,T=5K)$ in single-crystal $SrNiRu_5O_{11}$ with an in-plane current $\boldsymbol{J}$ and two directions of the applied magnetic field, $\boldsymbol{J} \perp \boldsymbol{H} \parallel \boldsymbol{c}$ and $\boldsymbol{J} \parallel \boldsymbol{H} \perp \boldsymbol{c}$ at $T = 5$ K (**Fig. 7**). In contrast to the Co-, Mn- or Fe-analogues **[6,11,18]**, we found no anomalous Hall signal in $SrNiRu_5O_{11}$, in that ρ_{xy} varies linearly on magnetic field applied in both directions. The negative slope of $\rho_{xy}(H)$ indicates that the dominant charge carriers in $SrNiRu_5O_{11}$ are electrons with a carrier concentration $n \approx 10^{21}$ cm^{-3} and mobility $\mu = R_0/\rho \approx 4.7\times 10^{-2} m^2V^{-1}s^{-1}$ at $T = 5$ K (using **Eq. 1** with $R_0 = d\rho_{xy}/dH = 1/nec$, where e is the electron charge and c is the speed of light). Note that the carrier concentration is one order of magnitude higher for $SrNiRu_5O_{11}$ than for Mn- or Co- bearing ferrites **[6,11]**, indicating the density of states $N(E_F)$ at the Fermi level increases when Co or Mn are replaced by Ni. The lack of an anomalous contribution to the Hall resistivity is highly significant, and suggests that any magnetic coupling developing below 130 K is probably limited to short-range correlations. Furthermore, the absence of a non-monotonic dependence of ρ_{xy} (which is linked to a possible THE **[6]**) and previous magnetic neutron scattering results on Mn- and Co-bearing ferrites **[10,11]**, argue against a canted variant of an in-plane, coplanar ''q = 0'' arrangement of Ru^{3+} ($S = ½$) spins residing on the Kagomé triangles in $SrNiRu_5O_{11}$.

The temperature dependence of the electrical resistivity of single-crystal $SrNiRu_5O_{11}$ with in-plane current $\boldsymbol{J} \perp \boldsymbol{H} \parallel \boldsymbol{c}$ is shown in **Fig. 8**. The compound exhibits metallic/semi-metallic

conductivity down to 4.5 K. The residual resistivity $\rho_o(T$=4.5 K) = 13.2 μΩ-cm indicates a reasonably good-quality sample. No significant difference is observed between measurements in zero field or 5 T. It is interesting that a near-linear temperature dependence of the in-plane resistivity persists over the high-temperature interval, 200 K – 300 K. The strong convexity of ρ(T) near 100 K is similar to the "saturating resistivities" of strongly paramagnetic actinide compounds **[19]**. This behavior also mimics high-temperature cuprate or iron-arsenide-based superconductors, where it is considered a signature of marginal Fermi liquid physics. As the temperature decreases below about 200 K, the resistivity gradually deviates from linearity, and exhibits a clear slope change near 70 K. A rapid decrease of the resistivity below 70 K suggests a cross-over between temperature-dependent scattering mechanisms of different types. Below 40 K, the resistivity can be fitted to a $T^{1.6}$-dependence, as shown in the inset of **Fig. 8**; this power law is a signature of scattering by strong spin fluctuations in metallic actinide and transition element materials that are nearly magnetic or weakly ferromagnetic **[19,20]**. In contrast, a T^2-dependence of the low-temperature electrical resistivity is predicted by Fermi liquid theory in the limit $T \rightarrow 0$ K. The reduction of the resistivity exponent below 2 is expected for an antiferromagnetic quantum critical point, since the strong scattering of electrons takes place at particular antiferromagnetic wavevectors ("hot spots") around the Fermi surface, allowing larger areas of the Fermi surface to ''short out'' this strong scattering with conventional Fermi liquid transport **[21]**. The deviation of the resistivity data from Fermi liquid behavior below 40 K is therefore consistent with NFL behavior, and also consistent with the temperature dependence of the magnetic susceptibility, which crosses over from a high-temperature Curie-Weiss to a divergent power-law behavior predicted by NFL models. In any case, it is clear that the transport and magnetic properties of $SrNiRu_5O_{11}$ cannot be explained within Fermi liquid theory.

3.3. Specific Heat

The inset in **Fig. 9** shows the temperature dependence of the specific heat of $SrNiRu_5O_{11}$, which reveals no anomalous behavior that could indicate phase transitions over the temperature range 0.35 – 50 K. The specific heat below 10 K has been analyzed by considering the electronic, lattice and nuclear Schottky contributions. The nuclear specific heat in $SrNiRu_5O_{11}$ can be attributed to Ru and Ni isotopes with non-zero quadrupole moment (i.e., having nuclear spin I > 1/2) residing at sites with axial symmetry and a non-zero electric field gradient. In addition, unpaired *d* electrons of Ru and Ni can generate magnetic hyperfine fields if the atomic spin relaxation is slower than the Larmor frequency of the nuclear spin **[22]**. We considered isotopes (with natural abundance 1.2% for ^{61}Ni, 12.76% for ^{99}Ru, and 17.06% for ^{101}Ru) that appreciably contribute to a nuclear Schottky effect arising from quadrupole and hyperfine interactions. We fitted our data below 10 K to the expression

$$C(T) = \gamma T^{\alpha} + \beta T^3 + D/T^2 \qquad \textbf{(2)}$$

where $C_{el} = \gamma T^{\alpha}$ is the electronic contribution, $C_{lat} = \beta T^3$ is the lattice contribution, and $C_{sch} = D/T^2$ represents the high-temperature form of the nuclear Schottky term. The standard fit using **Eq. 2** with $\alpha = 1$ was relatively poor, but was substantially improved using a phenomenological C_{el} term with exponent $\alpha = 1.2$ (**Fig. 9**). The best-fit coefficients are $\gamma = 0.134$ J/mol $K^{2.2}$, $\beta = 3.2 \times 10^{-4}$ J/mol K^4, and $D = 8.6 \times 10^{-4}$ J-K/mol. Note that a fit that includes only conventional Sommerfeld electronic and Debye phonon contributions yields similar coefficients, $\gamma = 0.144$ J/mol K^2 and $\beta = 6.5 \times 10^{-4}$J/mol K^4.

Both types of fit indicate a relatively large electronic contribution to the specific heat for a semimetal, but typical of moderately heavy fermion materials **[23]**. A possible heavy fermion state in $SrNiRu_5O_{11}$ would traditionally be attributed to hybridization between localized Ni-3d and Ru-4d conduction electron states. More generally, a large γ may indicate a substantial contribution from fluctuating magnetic moments in the system. The paramagnon model **[24–**

26] of spin fluctuations in exchange-enhanced paramagnets and nearly ferromagnetic materials predicts a heat capacity contribution of the form $T^3 \ln(T/T_{sf})$ to the electronic specific heat, where T_{sf} is a characteristic spin fluctuation temperature. However, all our attempts to include this term failed; and we therefore concluded that the fractional power law term most adequately describes the data. The calculated electronic contribution to the total specific heat divided by T versus temperature, according to the corrected **Eq. (2)** that includes $C_{el} = \gamma T^{1.2}$, is shown in **Fig. 10**, where it is clear the behavior of C/T for $T < 10$ K is not constant as in normal metals, but varies as $T^{0.2}$. In conventional metals $C_{el} \sim \gamma T$ at low temperatures and the clear deviation (taking into account a nuclear Schottky term to the total heat capacity) of the exponent α from unity is another indication of the unconventional character of the low-energy excitations in $SrNiRu_5O_{11}$.

Nevertheless, the unconventional power law dependence of $C_{el}(T)$ is consistent with that expected for the massless Dirac fermion states in topological insulators (TI), or gapless spin liquids realized on $S = ½$ Kagome nets **[27,28]**. In contrast, the low temperature electronic specific heat of $BaCo_2Ru_4O_{11}$, which is one of the lower-T_C magnetic phases of the R-type ferrite class, exhibits conventional $C_{el} \sim \gamma T$ behavior with a moderate $\gamma \approx 120$ mJ/mol K^2) **[4,29]**. The observed evolution of the specific heat as a function of the 3d-element suggests a transition from a "trivial" to "topological" behavior within the structural family of the ruthenium ferrites, which is driven by the 3d/4d element ratio---in other words, by the relative strength of spin-orbit (4d-element) and electron-electron (3d-element) interactions. The protection of the Dirac point by time reversal symmetry can be lifted by magnetic ordering, which takes place when Ni is substituted by Fe, Mn, or Co. As a result, a gap that separates the upper and lower branches of the Dirac cone is formed, leading to massive fermion states **[30]**. Note that a Kagomé lattice has been argued to play an essential role in the formation of a two-dimensional TI **[31]**. However, these scenarios are complicated by the presence of

substantial atomic disorder on the Kagomé lattice in the magnetically ordered R-type ferrite compositions studied to date.

Based on these results one may suggest that an intermediate topological Mott insulator state exists between the topological band insulators and the familiar Mott insulating phases for relatively strong electron-electron interactions for which magnetic ordering is expected. A model based on the slave-rotor approximation and the strong coupling limit **[27]** yields a phase diagram with four main phases whose stabilities depend upon the Hubbard repulsion U and spin-orbit coupling λ for moderately strong electron-electron repulsion: 1) metallic, 2) topological band insulator, 3) topological Mott insulator, and 4) gapless Mott insulator. The experimental data suggest that $SrNiRu_5O_{11}$ might be located somewhere near the boundary between the gapless Mott insulator and metallic states. It should be noted that in bulk TI samples **[32-34]**, the transport properties of the surface states are often mixed with those of bulk states, making it difficult to observe insulating behavior in ρ(T). The bulk conductivity decreases while the conductivity due to the surface states increases with decreasing temperature, and the electrical conduction at low temperature is dominated by the surface. The ρ(T) data of $SrNiRu_5O_{11}$ therefore could be interpreted to reflect metallic behavior that is similar to other bulk TI.

Alternatively, the enhanced Sommerfeld coefficient of $SrNiRu_5O_{11}$ and a metallic/semimetallic temperature dependence of the electrical resistivity are consistent with incipient band magnetism in this compound, suggesting that this material is an example of a frustrated system with a spin-liquid state that involves itinerant electrons. On the other hand, our observations of high values of the effective magnetic moment classify $SrNiRu_5O_{11}$ as a localized moment system. The relatively high Weiss temperatures (-150 K and -69 K for the two crystallographic orientations) and the absence of any magnetic order down to 0.4 K may also signal a spin-liquid state, as might be expected for the Kagome net of Ru^{3+} (S = ½) spins.

It is interesting to note that the $C_{el} = \gamma T^{\alpha}$ term with exponent α = 1.2-1.3 is observed in gapless spin liquids (e.g., herbertsmithite **[35]** and vanadium oxyfluoride **[36]**), where spin fluctuations persist down to T = 0 K due to the strong geometrical frustration present on the S = 1/2 Kagomé net. These insulating materials with highly localized magnetic moments show a near-linear specific heat that signals the thermal excitations are dominated by itinerant electrons at low temperatures. On the other hand, the physics of magnetic frustration in metallic systems is relatively unexplored, mainly due to the lack of model systems. A possible spin-liquid state has been detected in a few metallic materials that do not have a Kagomé net---e.g.,Y(Sc)Mn_2 with itinerant 3d-electron spins on a pyrochlore lattice **[37]**. Moreover, a number of frustrated metallic materials in a spin-liquid state exhibit a conventional linear specific heat C ~ T **[38]**.

Generally speaking, the non-analytic divergences in both heat capacity and magnetic susceptibility, together with a $T^{1.6}$-dependence of the electrical resistivity data, indicate that the system is on the verge of a magnetic phase transition that must occur below 0.35 K (our low-temperature limit in heat capacity experiments) in the case of $SrNiRu_5O_{11}$. Given the Ru moments lie on a frustrated Kagomé lattice, magnetic order is likely suppressed by quantum fluctuations above a highly degenerate quantum-spin-liquid ground state, which is one type of NFL state widely discussed in literature.

In the case of intermetallic compounds, current NFL theories can be divided into three general categories: multichannel Kondo models **[39]**, systems proximate to QCP treated by renormalization group theory of spin fluctuations **[40]**, and models based on atomic disorder **[41]**. Our magnetic susceptibility and electrical resistivity data for $SrNiRu_5O_{11}$ show that these NFL models do not adequately describe our data, for the following reasons: 1) Three-dimensional renormalization group theory for well-ordered materials near a QCP predicts $\chi \sim T^{3/2}$, $\rho \sim T^{3/2}$ (AFM QCP) or $\rho \sim T^{5/3}$ (FM QCP); 2) the multichannel Kondo or Kondo

disorder models demand $\chi \sim -\ln T$ and $\rho \sim 1 - aT$; 3) models of Kondo alloys require atomic disorder and large residual resistivities **[41]**. These models do not provide self-consistent agreement with our resistivity and susceptibility data, and the fact that the residual ($T = 0$) resistivity of our single crystal is 13.2μΩ cm (which indicates a well-ordered, clean sample). Moreover, $SrNiRu_5O_{11}$ has no significant homogeneity range and is structurally ordered, according to our single-crystal structure refinements **[8]**. We conclude that an alternative NFL mechanism is needed to explain the observed low temperature behavior of the magnetic, transport and thermodynamic properties of $SrNiRu_5O_{11}$.

Note, that the above-cited NFL theories have been developed for f-electron, heavy fermion intermetallics, the magnetic and electronic properties of which are dictated by interactions between localized f-orbitals with strong magnetic moments and itinerant electrons. In some cases, transition metal oxides also behave as heavy fermion metals **[42-44]** if a paramagnetic state survives at low temperatures due to geometrical frustration **[45]**. Furthermore, in metallic systems magnetic order can be suppressed by frustrated interactions or by conduction electron screening through the Kondo effect. The *combination* of strong geometrical frustration and Kondo screening leads to a phase transition into a quantum-spin-liquid state that persists to very low temperatures (see **[38]** and references therein).

It is instructive to view $SrNiRu_5O_{11}$ as an ordered example of the R-type ferrites with strong magnetic frustration generated within the ***ab***- (Kagomé) nets. In contrast, the isostructural, metallic Co- (T_C = 105 K) and Mn- (T_C = 183 K) ferrites suffer from substantial 3d/4d disorder on M(2) sites within the Kagomé nets **[6, 11]**. Consequently, the magnetic frustration is depressed, and long-range ferromagnetic ordering occurs at remarkably high temperatures **[4]**. In the case of $SrNiRu_5O_{11}$, the structural disorder in the Kagomé planes is absent. Furthermore, in ferrites where Co and Mn are completely replaced by Ni and Ru, the electrons become more itinerant, most probably due to an increased density of electrons and

reduction of disorder in the system. Therefore, the magnetic frustration and orbital degeneracy are hard to remove, and no magnetic ordering is observed in $SrNiRu_5O_{11}$. However, the spin and orbital degrees of freedom of Ni are both evident from the sizable magnetization and Curie-Weiss behavior. Therefore, the Ni spins may order as temperature is lowered below 1 K, for example, via long-range dipole interactions. In this situation, we expect the competition between magnetic correlations among Ni^{2+}magnetic moments and geometrical frustration on the Kagomé nets to play an essential role in the precise nature of the ground state of $SrNiRu_5O_{11}$. In summary, the geometrical frustration and antiferromagnetic correlations within the Ru^{3+} (S = ½) triangular lattice result in very large ground state degeneracy with no long-range order at any temperature, while the remaining interactions between the Ni^{2+} spins tend to order the system ferromagnetically. If these two processes are about equal in strength, then $SrNiRu_5O_{11}$ might lie near a spin-liquid phase transition.

4. Conclusion

We observe a highly unusual combination of magnetic, transport and thermal behaviors of single-crystal $SrNiRu_5O_{11}$. We speculate that an important role in the formation of this unusual ground state is played by competition between weakly interacting Ni^{2+} (S = 1) spins located between two-dimensional Kagomé layers, and geometrically frustrated Ru^{3+} (S = ½) spins located within the Kagomé nets. Although the compound does not show a clear signature of long-range magnetic order down to 0.35 K, residual magnetic Ni–Ni interactions induce a small non-linear field dependence of magnetization at low temperatures. The Hall resistivity reveals no anomalous contribution down to 4.5 K, consistent with the absence of ferromagnetism. The power law dependence of the electronic specific heat suggests a spin-liquid or TI state with massless Dirac fermions. The existence of exotic low-energy

excitations at low temperatures might originate from the topological character of the tight binding band structure of a Kagomé lattice **[31]**.

Acknowledgements

We thank Ingrid Werner for performing the microprobe measurements and Dr.Shiyu Zhang for experimental support. We thank R. K. Kremer for heat capacity measurements. Research at the University of Kentucky was supported by the U.S. Department of Energy Grant No. DE-FG02-97ER45653.

References

1. R. J. Cava, Dalton Trans. **19**, 2979-2987 (2004), and references therein.
2. Gang Cao and Lance E. De Long, Eds., *Frontiers of 4d- and 5d-Transition Metal Oxides* (Singapore, World Scientific Publishing, 2013; ISBN 978-981-4374-85-9), Chapter 1.
3. B. Schüpp-Niewa, L. Shlyk, S. Kryukov, L. De Long, R. Niewa, Z. Naturforsch. **62b**, 753-758 (2007).
4. L. Shlyk, S. Kryukov, B. Schüpp-Niewa, R. Niewa, L. E. De Long, Adv. Mater. **20**, 1315-1320 (2008).
5. L. Shlyk, L. E. De Long, S. Kryukov, B. Schüpp-Niewa, R. Niewa, J. Appl. Phys. **103**, 07D112 (2008).
6. L. Shlyk, S. Parkin, L. E. De Long, Phys. Rev. B **81**, 014413 (2010).
7. L. Shlyk, S. Parkin, L. E. De Long, J. Appl. Phys. **107**, 09E109 (2010).
8. L. Shlyk, S. Strobel, Th. Schleid, R. Niewa, Z. Kristallogr. **227** 545-551 (2012).
9. L. Shlyk, S. Strobel, E. Rose, R. Niewa, Solid State Sci. **14**, 281-286 (2012).
10. M. L. Foo, Q. Huang, J. W. Lynn, W.-L. Lee, T. Klimczuk, I. S. Hagemann, N. P. Ong, R. J. Cava, J. Solid State Chem. **179**, 563-572 (2006).

11. L. Shlyk, B. G. Ueland, J. W. Lynn, Q. Huang, L. E. De Long, S. Parkin, Phys. Rev. B **81**, 184415 (2010).

12. J. D. Lee, in: *Concise Inorganic Chemistry*, Fifth Edition (Blackwell Science Ltd., Oxford, U.K., 1996).

13. G. R. Stewart, Rev. Mod. Phys. **73**, 797-855 (2001).

14. R. Karplus and J. M. Luttinger, Phys. Rev. **95**, 1154-1160 (1954).

15. L. Berger, Phys. Rev B **2**, 4559-4566 (1970).

16. Y. Taguchi, Y. Oohara, H. Yoshizawa, N. Nagaosa, Y. Tokura, Science **291**, 2573-2576 (2001).

17. N. Nagaosa, J. Sinova, S. Onoda, A. H. MacDonald, N.P. Ong, Rev. Mod. Phys. **82**, 1539 (2010).

18. L. Shlyk, R. Niewa and L. E. De Long, Phys. Rev. B **82**, 134432 (2010).

19. T. Moriya, *Spin Fluctuations in Itinerant Electron Magnetism* (Berlin, Springer-Verlag, 1985), Chapter 5.

20. M. B. Brodsky, A. J. Arko, A. R. Harvey and W. J. Nellis, in: A. J. Freeman and J. B. Darby, Jr., Eds., *The Actinides: Electronic Structure and Related Properties* (New York, Academic Press, 1974), Volume II, Chapter 5.

21, L. B. Ioffe, A. J. Millis, Phys. Rev. B **51**, 16151-16158 (1995).

22. O.V. Lounasmaa, *Hyperfine Interactions* (New York, Academic Press, 1967).

23. L. E. De Long, Phys. Rev. B **33**, R3556 (1986).

24. N. F. Berk and J. R. Schrieffer, Phys. Rev. Lett. **17**, 433 (1966).

25. S. Doniach and S. Engelsberg, Phys. Rev. Lett. **17**, 750 (1966).

26. M. J. Rice, Phys. Rev. **159**, 153 (1967).

27. D. Pesin and L. Balents, Nature Phys. **6**, 376 (2010).

28. Y. Ran, M. Hermele, P. A. Lee, X.-G. Wen, Phys. Rev. Lett. **98**, 117205 (2007).

29. L. Shlyk *et al.,* unpublished.

30. Y. L. Chen et al., Science **329**, 689 (2010).

31. H.-M. Guo and M. Franz, Phys. Rev. B **80**, 113102 (2009).

32. P. Dutta, D. Bhoi, A. Midya, N. Khan, P. Mandal, S. Shanmukharao Samatham, and V. Ganesan, Appl. Phys. Lett. **100**, 251912 (2012).

33. N. P. Butch, K. Kirshenbaum, P. Syers, A. B. Sushkov, G.S. Jenkins, H. D. Drew, and J. Paglione, Phys. Rev. B **81**, 241301(R) (2010).

34. Z. Ren, A. A. Taskin, S. Sasaki, K. Segawa, and Y. Ando, Phys. Rev. B **84**, 165311 (2011).

35. M. A. de Vries *et al*, Phys. Rev. Lett. **100**, 157205 (2008).

36. L. Clark *et al*, Phys. Rev. Lett. **110**, 207208 (2013).

37. M. Shiga, K. Fujisawa, and H. Wada, J. Phys. Soc. Japan. **62**, 1329 (1993).

38. C. Lacroix, J. Phys. Soc. Japan. **79**, 011008 (2010).

39. D. L. Cox and M. Jarrell, J. Phys. Condens. Matter **8**, 9825-9853 (1996).

40. A. J. Millis, Phys.Rev. B **48**, 7183-7196 (1993).

41. E. Miranda, V. Dobrosavljevic and G. Kotliar, J. Phys. Condens. Matter **8**, 9871-9900 (1996).

42. S. Kondo *et al*., Phys. Rev. Lett. **78**, 3729-3732 (1997).

43. C. Urano, M. Nohara, S. Kondo, F. Sakai, H. Takagi, T. Shiraki and T. Okubo, Phys. Rev. Lett. **85**, 1052-1055 (2000).

44. A. Krimmel, A. Loidl, M. Klemm, S. Horn and H. Schrober, Phys. Rev. Lett. **82**, 2919-2922 (1999).

45. M. S. Laad, L. Craco and E. Müller-Hartmann, Phys. Rev. B **67**, 033105 (2003).

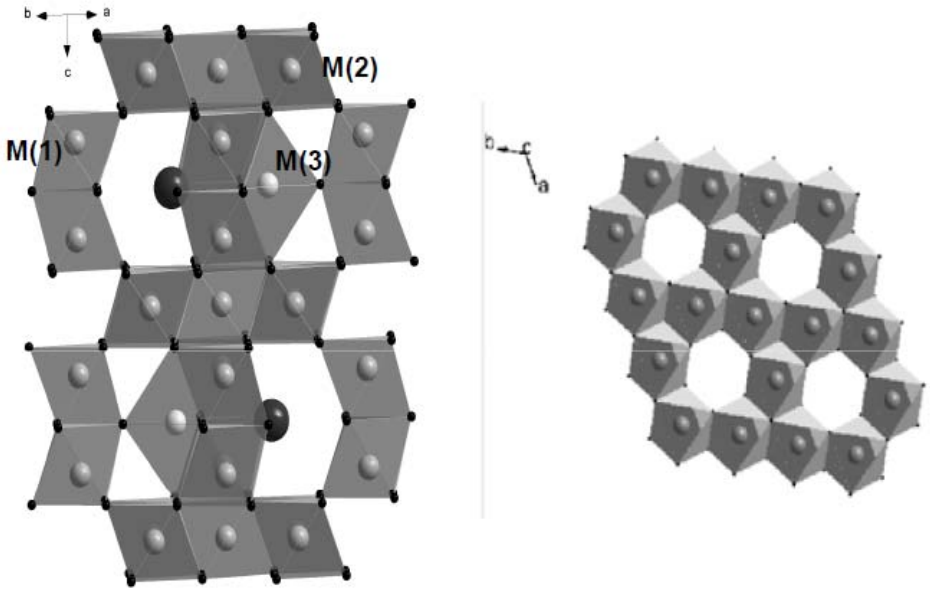

Fig. 1

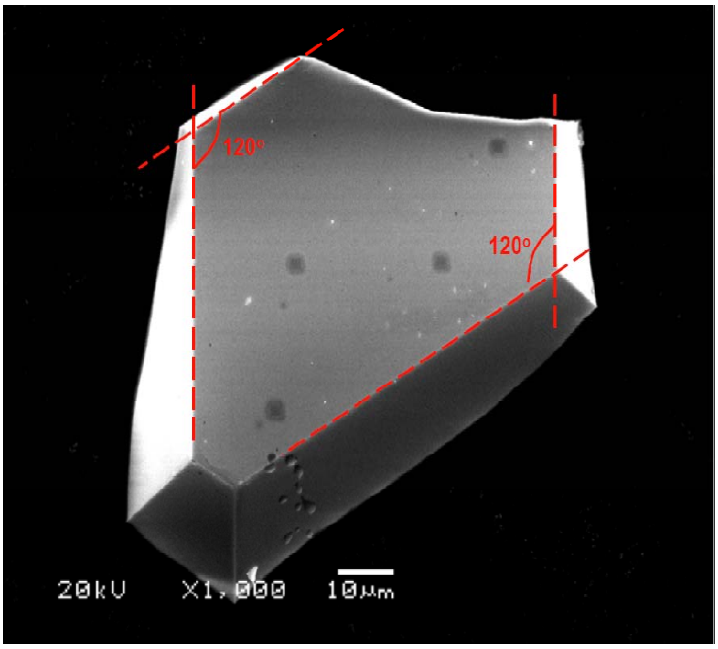

Fig. 2

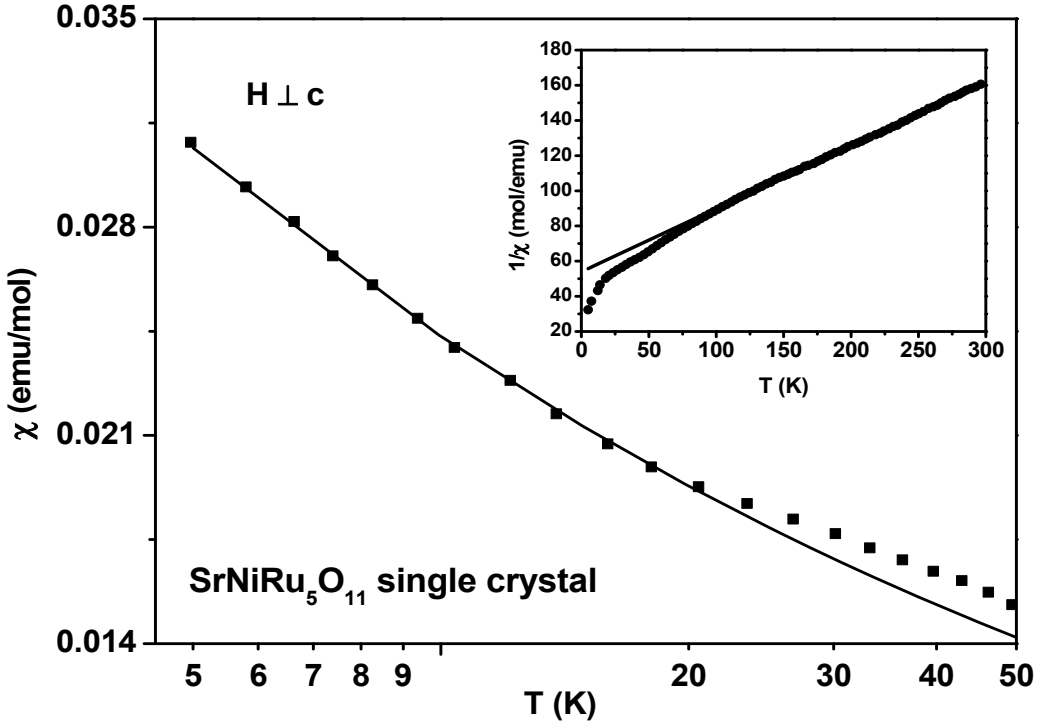
0.035
0.028
0.021
0.014
χ (emu/mol)
H ⊥ c
SrNiRu5O11 single crystal
5
6
7
8
9
20
30
40
50
T (K)
180
160
140
120
100
80
60
40
20
1/χ (mol/emu)
0
50
100
150
200
250
300
T (K)

Fig. 3

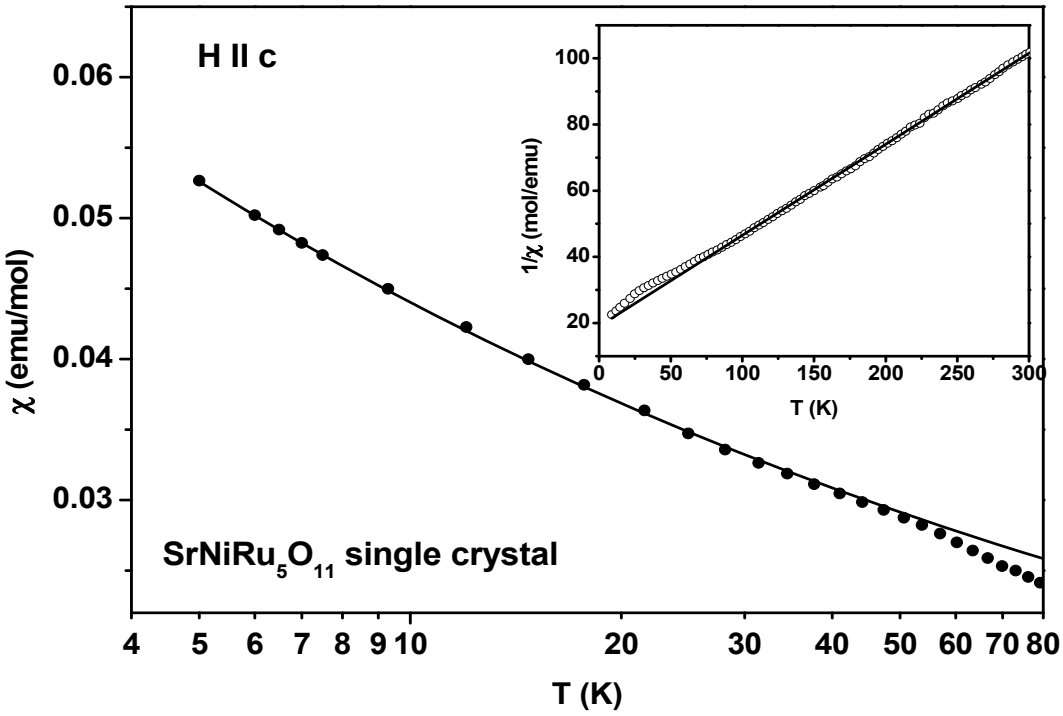
H ll c
0.06
0.05
0.04
0.03
χ (emu/mol)
SrNiRu5O11 single crystal
4 5 6 7 8 9 10 20 30 40 50 60 70 80
T (K)
100
80
60
40
20
1/χ (mol/emu)
0 50 100 150 200 250 300
T (K)

Fig. 4

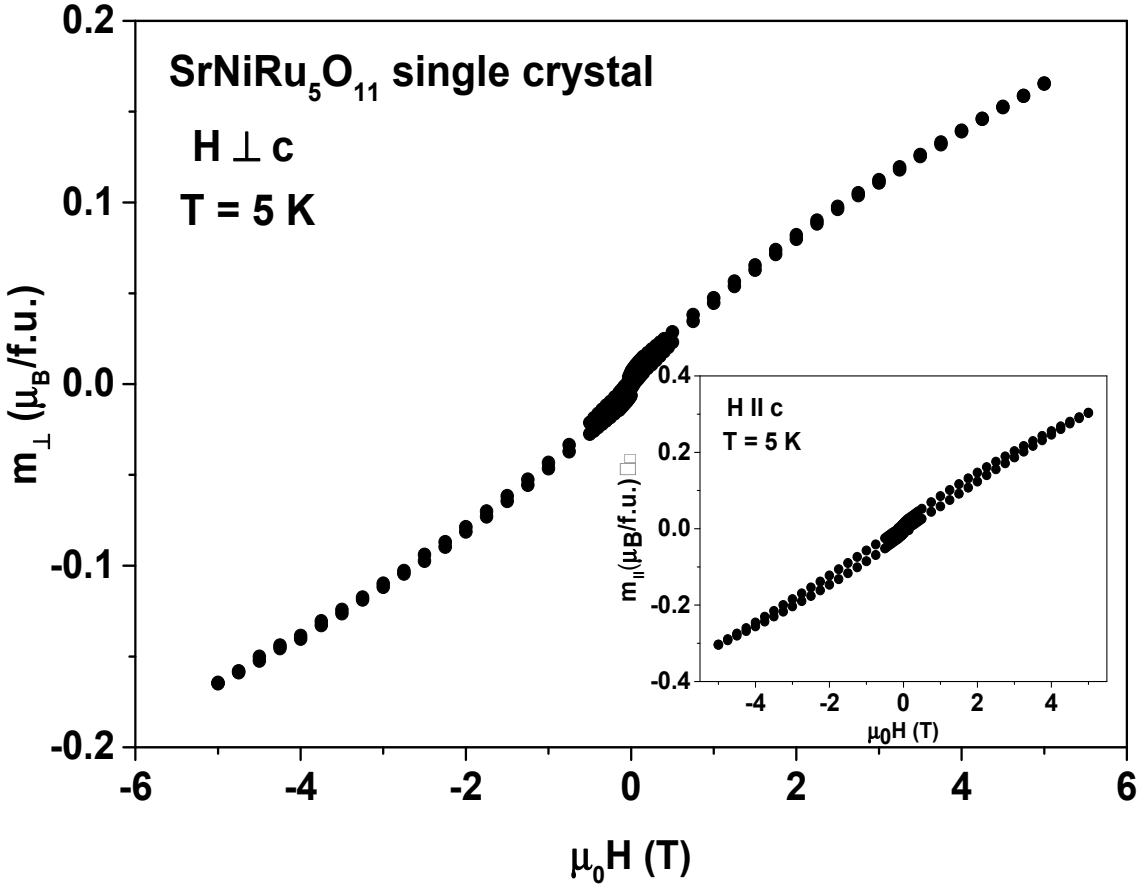
SrNiRu5O11 single crystal
H ⊥ c
T = 5 K
m⊥ (μB/f.u.)
μ0H (T)
H II c
T = 5 K
mII(μB/f.u.)
μ0H (T)

Fig. 5

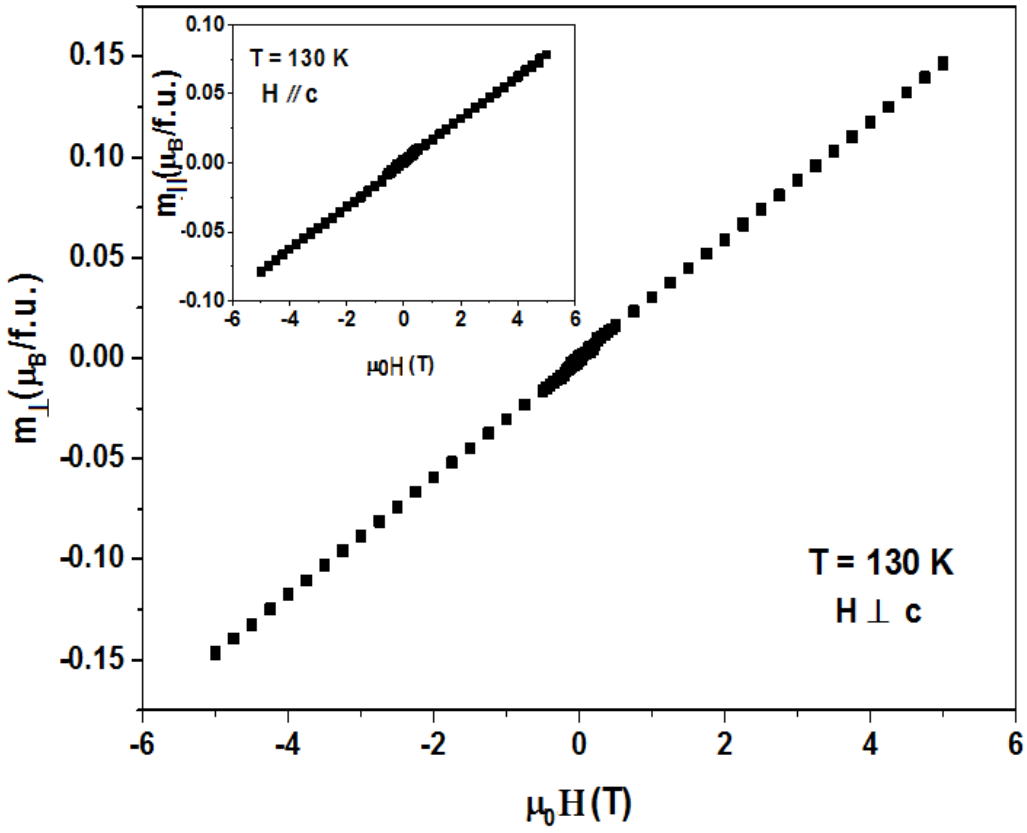

Fig. 6

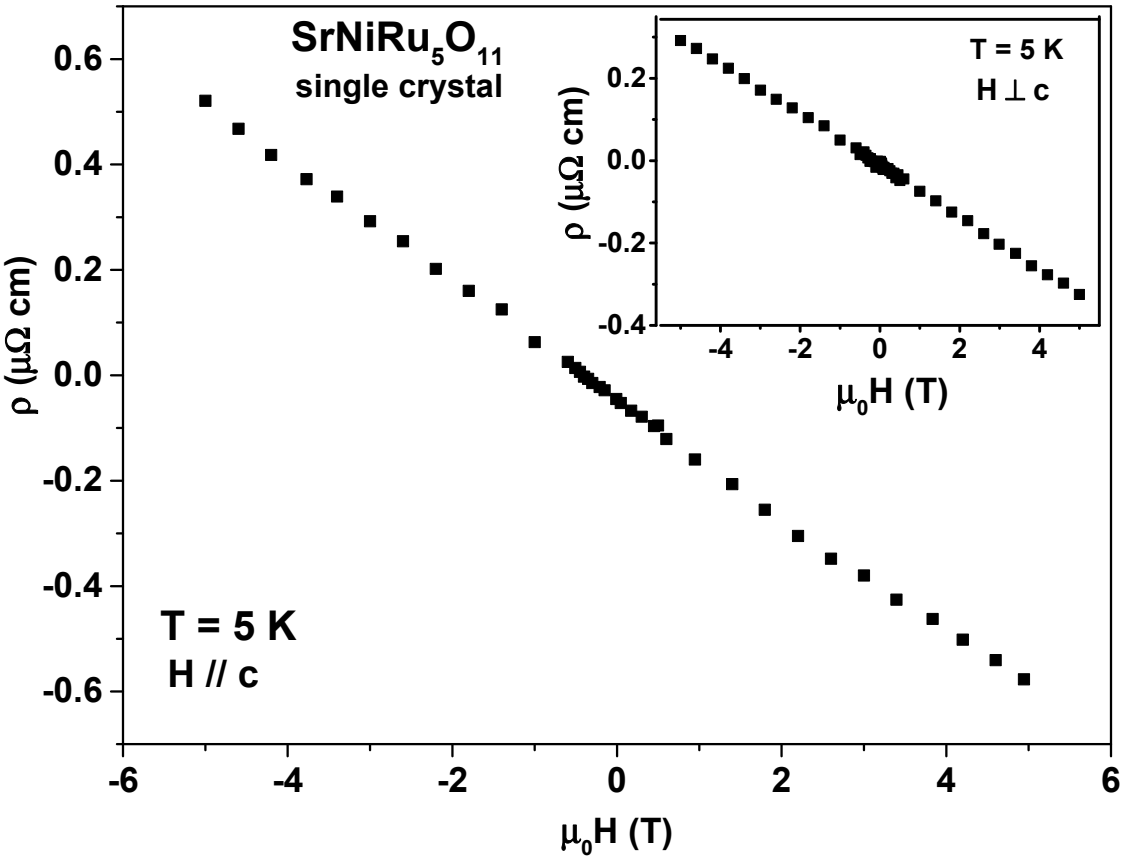
SrNiRu5O11
single crystal
T = 5 K
H // c
ρ (μΩ cm)
μ0H (T)
T = 5 K
H ⊥ c
ρ (μΩ cm)
μ0H (T)

Fig. 7

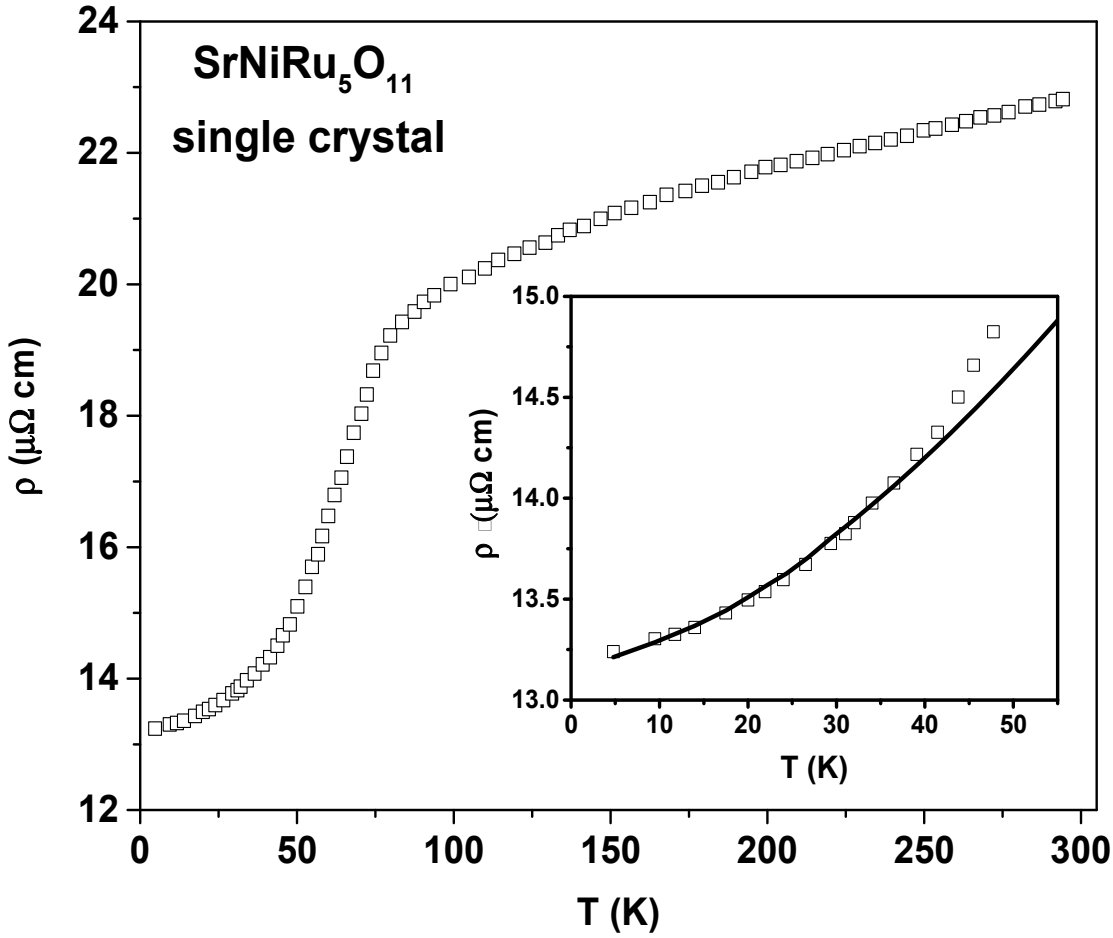
SrNiRu5O11
single crystal
ρ (μΩ cm)
T (K)
24
22
20
18
16
14
12
0
50
100
150
200
250
300
15.0
14.5
14.0
13.5
13.0
0
10
20
30
40
50

Fig. 8

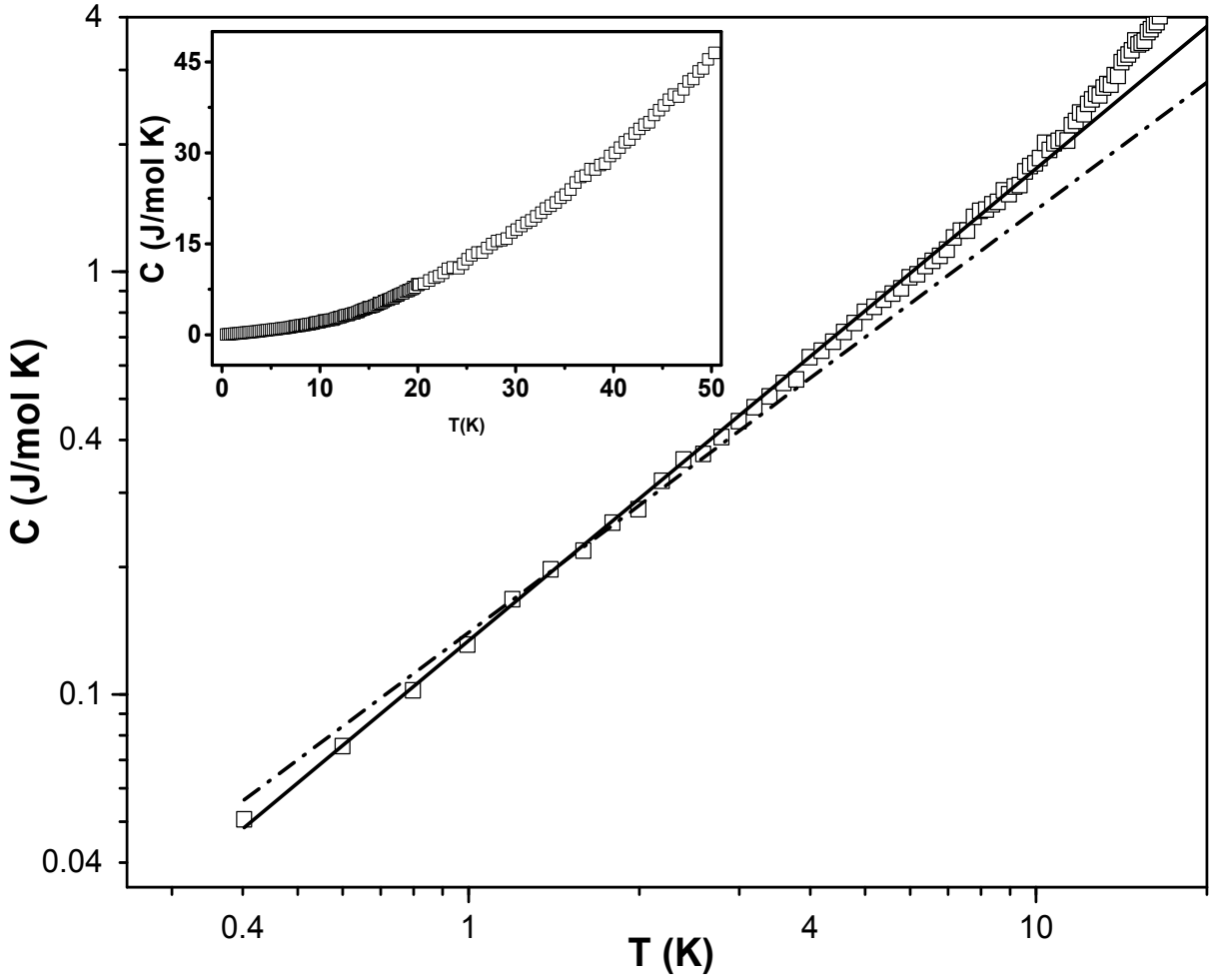

Fig. 9

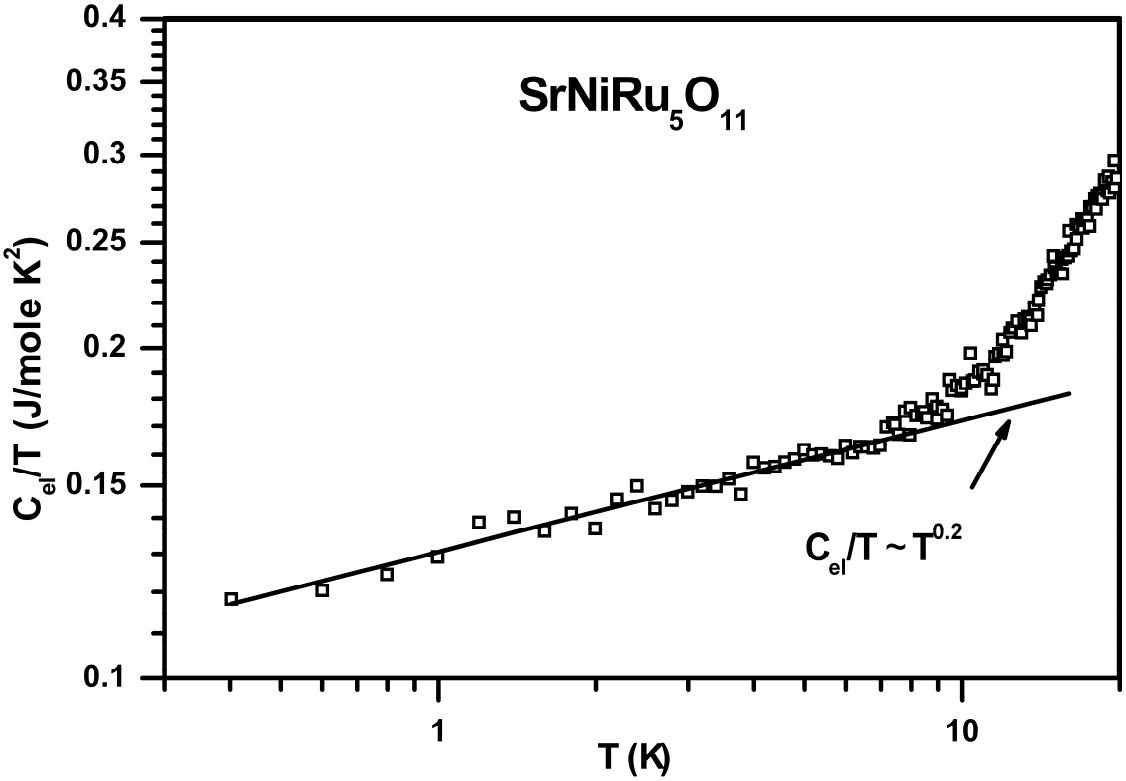
SrNiRu5O11
0.4
0.35
0.3
0.25
0.2
0.15
0.1
Cel/T (J/mole K2)
1
10
T (K)
Cel/T ~ T0.2

Fig. 10

Figure Captions

Fig. 1. Left panel: Crystal structure of $SrNiRu_5O_{11}$. Dark dots are oxygen atoms and large grey spheres are transition elements (Ru or Ni). The M(1) (4e) sites in face-shared octahedra, as well as M(2) (6g) sites in edge-shared octahedra in the Kagomé sublattice, are both occupied by Ru. The M(3) (2d) sites in double trigonal prisms are exclusively occupied by Ni. Dark spheres are Sr sites. **Right panel:** Arrangement of edge-sharing coordination polyhedra of transition metal ions in the ***ab*-** (Kagomé) plane.

Fig. 2. SEM image of a small crystal of $SrNiRu_5O_{11}$, revealing a hexagonal crystal habit, as shown by the characteristic angles highlighted by red dashed lines.

Fig. 3. Low-temperature magnetic susceptibility for field $\mu_o H = 0.5$ T applied perpendicular to the ***c*-**axis, $\chi_\perp$, versus temperature T. The solid curve is a fit to $\chi_\perp \sim T^{-0.3}$. **Inset:** The inverse magnetic susceptibility $(\chi_\perp)^{-1}$ versus T; the solid curve is a fit of the data to the Curie–Weiss law (see text for details).

Fig. 4. Low temperature magnetic susceptibility for magnetic field $\mu_o H = 0.5$ T applied parallel to the ***c*-**axis, $\chi_{/\!/}$ versus temperature T. The solid curve is a fit to $\chi_{/\!/} \sim T^{-0.3}$. **Inset:** The inverse magnetic susceptibility $(\chi_{/\!/})^{-1}$ versus T; the solid curve is a fit of the data to the Curie –Weiss law (see text for details).

Fig. 5. Magnetic moment $m_{\perp}$ perpendicular to the ***c*-**axis versus magnetic field H at temperature T = 5 K. **Inset:** The magnetic moment $m_{//}$ along the ***c*-**axis versus magnetic field at T = 5 K.

Fig. 6. Magnetic moment for applied field ***H*** perpendicular to the ***c*-**axis, $m_{\perp}$, versus H at temperature T = 130 K. **Inset:** The moment for ***H*** perpendicular to the ***c*-**axis, $m_{||}$, versus H at T = 130 K.

Fig. 7. Transverse resistivity ρ_{xy} versus magnetic field ***H*** || ***c***–axis for single-crystal $SrNiRu_5O_{11}$ at temperature T = 5 K. **Inset:** The transverse resistivity ρ_{xy} versus magnetic field ***H*** ⊥ ***c***-axis for single-crystal $SrNiRu_5O_{11}$ at T = 5 K.

Fig. 8. Temperature dependence of the longitudinal electrical resistivity $\rho = \rho_{xx}$ of single-crystal $SrNiRu_5O_{11}$ with in-plane current ***J*** ⊥ ***c***-axis. **Inset:** The low-temperature resistivity, where the solid curve is a fit of the data to $\rho_{xx} \sim T^{1.6}$.

Fig. 9. Low-temperature specific heat $C(T)$ of single-crystal $SrNiRu_5O_{11}$ versus temperature T (note logarithmic scale). The dashed line is a fit of the data to **Eq. (2)** with power law exponent α = 1.0. The solid line is an improved fit using **Eq. (2)** with a modified electronic contribution, $C_{el} = \gamma T^{1.2}$. Inset shows the total specific heat $C(T)$ data for single-crystal $SrNiRu_5O_{11}$ over the temperature range 0.35 K to 50 K.

Fig. 10. Calculated electronic contribution to the specific heat C_{el} derived from the best fit of the total specific heat versus temperature, determined from the following procedure: First we

obtain the best-fit description of the total specific heat data using $C(T) = \gamma T^{1.2} + \beta T^3 + D/T^2$, where the form of the first term is attributed to spin-liquid behavior **[35,36]**. Second, the electronic contribution was separated as a difference between the total heat capacity and the sum of nuclear Schottky and lattice contributions: $C_{el}(T) = C_{total}(T) - (\beta T^3 + D/T^2)$. We show not C_{el}, but C_{el}/T, in order to emphasize how the coefficient $\gamma \equiv C_{el}/T$ from a traditional Sommerfeld fit must decrease at the lowest temperatures, which differs from the constant value observed for conventional metals. The solid line is shown to demonstrate that C_{el}/T follows to a $T^{0.2}$-law below 10 K. Note that the data are shown as a log-log plot.